Magnetic and neutron diffraction studies of long-range ferromagnetic order in monolayered manganites

Chang Seop Hong,[1] Wan Seop Kim,[1] Nam Hwi Hur,[1,*] and Yong Nam Choi[2]
[1]*Center for CMR Materials, Korea Research Institute of Standards and Science, Yusong, P.O. Box 102, Daejon 305-600, Korea*
[2]*Neutron Physics Department, Korea Atomic Energy Research Institute, Yusong, P.O. Box 105, Daejon 305-600, Korea*
(Received 1 May 2003; published 27 August 2003)

The structural, magnetic, and electrical properties of single crystals of Ru-doped monolayered manganites $La_{0.5}Sr_{1.5}Mn_{1-x}Ru_xO_4$ ($0 \leqslant x \leqslant 0.5$) were investigated by neutron-diffraction, magnetization, and transport measurements. With increasing Ru content, the magnetic ground state changed from the parent antiferromagnetic (AFM) to the spin-glass to the ferromagnetic (FM) phase. The temperature-dependent neutron-diffraction measurements at $x=0.35$ clearly revealed long-range FM order in the monolayered manganite, which was confirmed by bulk magnetometry. The uniaxial magnetic anisotropy, in which the Ru spins are aligned along the *c* axis, was also observed in the compounds. This unique magnetic behavior might be ascribed to the magnetic anisotropy of the Ru ions stabilized under the structural distortion, as well as the FM ordering of Mn spins induced by AFM coupling among Mn/Ru pairs. The magnetoresistance of the Ru-doped system, which exhibits conduction confinement within a layer, diminishes with increasing Ru doping because of an increase in the proportion of FM domains at the expense of the magnetic glassy state.

DOI: 10.1103/PhysRevB.68.064425 PACS number(s): 75.25.+z, 75.47.Gk, 75.50.Lk

I. INTRODUCTION

Recent resurgent interest in perovskite manganites, which is the $n=\infty$ member of the Ruddlesden-Popper series $A_{n+1}Mn_nO_{3n+1}$, is mainly attributed to their unique magneto transport phenomenon, known as colossal magnetoresitance (CMR).[1–6] The CMR effect occurs in the vicinity of the long-range ferromagnetic(FM) ordering temperature T_C associated with spin, charge, and lattice degrees of freedom. Within the double-exchange (DE) picture, based on the FM interaction between Mn^{3+} and Mn^{4+} ions, the essential factor driving CMR is the Mn 3*d* electrons. Accordingly, the introduction of a foreign element into the Mn site is a good way to control and alter the intrinsic physical properties of the parent material. For instance, Cussen *et al.* found that substitution of diamagnetic Ga^{3+} into the $RMnO_3$ phase (R =La, Nd) strongly affected both the crystal structure and resulting magnetic ordering.[7] In the Cr-doped manganite $LaMn_{1-x}Cr_xO_3$, where Cr^{3+} is introduced solely into the Mn^{3+} site, the DE interaction is induced via the Mn^{3+}-O-Cr^{3+} couple.[8] For the $n=1$ member La_4LiMnO_8 and $La_3SrLiMnO_8$, the cation ordering and magnetic behavior are very complicated and the transition-metal centers interact magnetically in a manner that can be explained by the superexchange mechanism.[9]

Long-range FM and AFM(antiferromagnetic) interactions are theoretically absent in one- (1D) and two-dimensional (2D) isotropic systems based on Heisenberg models.[10] In a real material having a low-dimensional structure, however, several factors (such as interchain/interlayer magnetic interaction and magnetic anisotropy) drive long-range magnetic order at a finite temperature.[11] Within this context, the long-range FM and/or AFM ordering can be produced in the monolayered manganite by tuning various ingredients,[12] as exemplified in $La_{0.5}Sr_{1.5}MnO_4$, which shows a CE-type AFM ordering near 110 K.[13] On the other hand, a real long-range FM order at zero field has not been discovered yet in the $n=1$ member, although the FM interaction itself has been observed in the polycrystalline Ru-doped samples with the formula of $La_{0.5}Sr_{1.5}Mn_{1-x}Ru_xO_4$ ($0 \leqslant x \leqslant 0.15$). A FM moment induced by Ru doping has been confirmed by magnetization measurements, but no long-range FM order has been observed.[14] Very recently, Battle *et al.* identified the presence of a spin-glass phase at zero field in Rh-doped manganite $La_{0.8}Sr_{1.2}Mn_{0.6}Rh_{0.4}O_4$, as well as long-range FM ordering under an applied magnetic field, which they ascribed to the subtle change in band structure brought about by the magnetic field.[15]

Of particular interest at present is whether or not real long-range FM ordering exists in the monolayered manganites. Previous work has shown that the magnetic anisotropy of Pr and Nd ions in $R_{1-x}Sr_{1+x}MnO_4$ (R=La, Pr, Nd), stabilized by structural anisotropy, influences the Mn spins more significantly along the *c* axis than in the *ab* plane.[16,17] This study prompted investigation of the direct substitution of a foreign element exhibiting magnetic anisotropy into the Mn site of the monolayered manganite, with the hope that it might induce long-range FM ordering. A Ru-doped system was chosen to verify this postulate, mainly because Ru also collapses the parent AFM state and induces a FM moment. It is worth mentioning that paramagnetic $CaRuO_3$ can be made ferromagnetic by partial substitution of Ru by Ti.[18] An attempt has been made to grow single crystals in order to extend the Ru doping concentration and further explore this issue.

This paper reports on the structural, magnetic, and transport properties of single crystals of $La_{0.5}Sr_{1.5}Mn_{1-x}Ru_xO_4$ ($x=0.0$, 0.1, 0.2, 0.35, 0.5). The main purpose of this paper is to present clear evidence of long-range FM order at zero magnetic field in the monolayered manganite, as observed in the $n=2$ and ∞ members. This Ru-induced FM ordering appears to be associated with magnetic anisotropy, in which

the Ru spins are aligned along the *c* axis. In addition, the paper also discusses the magnetoresistance (MR), which lessens with increasing Ru doping.

II. EXPERIMENTAL SECTION

Polycrystalline powders of $La_{0.5}Sr_{1.5}Mn_{1-x}Ru_xO_4$ ($x=0.1$, 0.2, 0.35, 0.5) were prepared using the conventional solid-state reaction method. Stoichiometric amounts of dried La_2O_3, $SrCO_3$, MnO_2, and RuO_2 were weighed and mixed thoroughly in an agate mortar. The mixed powders were heated at 1000 °C for 5 h in air. After calcination, the powders were pelletized and sintered at 1450 °C for 10 h. The resulting pellet was ground to powder, which was then cold pressed to make a cylindrical rod (6 mm×80 mm=diameter ×length). The rod was fired at 1450 °C for 10 h in air. Single crystals of $La_{0.5}Sr_{1.5}Mn_{1-x}Ru_xO_4$ ($x=0.1$, 0.2, 0.35, 0.5) were grown under an oxygen atmosphere using a floating-zone image furnace equipped with four mirrors and four halogen lamps, and having a total input power of 4 kW. The oxygen flow rate was 3.0 l/min and the growth rate was 18 mm/h. Both feed and seed rods were coaxially rotated in opposite directions at a rate of 25 rpm. A single crystal with $x=0.0$ was grown according to methods reported previously.[16]

Crystals from the boule were crushed into powder for both x-ray and neutron-diffraction measurements. X-ray diffraction (XRD) was performed using a Rigaku diffractometer equipped with Cu$K\alpha$ radiation. Neutron-diffraction data were taken over the 2θ range of 0°–160°, with a step size of 0.05°, on a high-resolution powder diffractometer at HANARO Center in KAERI using a neutron source of $\lambda=1.8348$ Å supplied by a Ge(331) single-crystal monochromator. The ground crystalline samples were loaded into a vanadium can (diameter=12 mm, length = 45–55 mm), which was then placed in a helium-filled Al shield for variable-temperature experiments. Rietveld refinement of diffraction data was carried out using the FULLPROF program, employing a pseudo-Voight peak shape function. For $x=0.5$, negligible amounts of $La(OH)_3$ and La_2O_3 impurities were detected in the profile analysis. The chemical compositions for the Ru-doped crystals were determined from electron probe microanalysis (EPMA) and neutron diffraction. For magnetic and transport measurements, fine single crystals were sorted out by cleaving the multicrystal boule (5 mm in diameter ×50 mm in length). The cleaved surface was identified as the *ab* plane, as determined by XRD. Measurements of both the magnetization and transport characteristics were made using a quantum design MPMS-5 SQUID (superconducting quantum interference device) magnetometer, with magnetic fields applied either parallel to the *ab* plane or along the *c* axis. The resistance was measured as a function of temperature using the standard four-probe method with and without a magnetic field. The four-point contacts were made with molten indium deposited on the crystal sample surface.

III. RESULTS AND DISCUSSION

For the crystal growth of the Ru-doped manganite, much care needed to be taken due to the evaporation of ruthenium in the growth process. The maximum growth rate, about 18 mm/h, was employed to minimize Ru loss. Successful crystal growth was accomplished using a seed crystal with the same K_2NiF_4-type structure. It has been known that polycrystalline samples of $La_{0.5}Sr_{1.5}Mn_{1-x}Ru_xO_4$ have a low solubility of Ru ($x<0.20$).[14] However, using the floating-zone technique it is feasible to extend this solubility limit by up to 41%. This high solubility achievable in single crystals is likely due to facile interdiffusion between the Ru and Mn ions in the melted liquid zone.

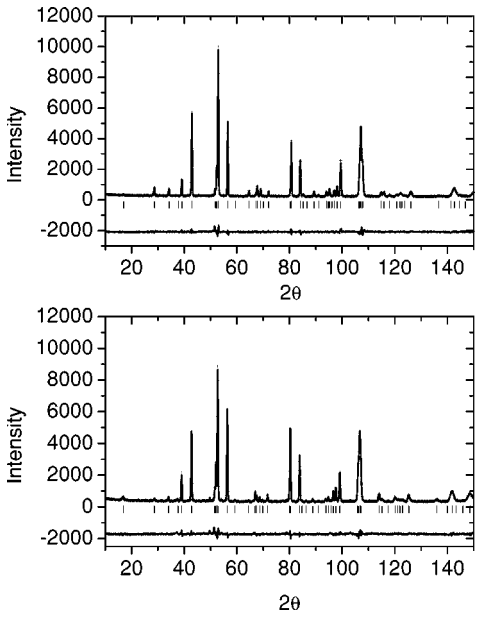

FIG. 1. Observed, calculated, and difference neutron-diffraction profiles at 300 K for $x=0.2$ (top panel) and 0.5 (bottom panel) in $La_{0.5}Sr_{1.5}Mn_{1-x}Ru_xO_4$. Agreement indices are presented in Table I.

The neutron powder-diffraction data at 300 K for all the Ru-doped compounds are well indexed with the tetragonal $I4/mmm$ symmetry. Refinements with similar lattice constants to $La_{0.5}Sr_{1.5}MnO_4$ based on this space group led to good agreement between the observed and calculated diffraction patterns, indicating long-range disordering of the Mn and Ru ions. Examples of the Rietveld fit are shown in Fig. 1 for samples of composition $x=0.2$ and 0.5. Ru defects in the Mn/Ru sites were observed in all Ru-doped samples. The refined occupancy of the Ru cation is found to be 0.09(1) at $x=0.1$, 0.17(1) at $x=0.2$, 0.30(1) at $x=0.35$, at 0.41(1) for $x=0.5$, consistent with the EPMA results. The other atoms virtually maintain their nominal compositions within experimental error. Structural parameters for all the samples at 10 and/or 300 K are summarized in Table I. From the structural data at 300 K, lattice parameters are seen to expand with increasing *x*. Given that Ru^{4+} (radius=0.62 Å)/Ru^{5+} (radius =0.57 Å) exists in Ru-doped perovskite compounds,[19] this result suggests that Ru atoms largely substitute into the smaller Mn^{4+} (radius=0.53 Å) rather than the larger Mn^{3+} sites (radius=0.65 Å).

Temperature-dependent neutron-diffraction experiments were performed for the $x=0.1$ and 0.35 samples. Figure 2 displays the lattice parameters and cell volumes for $x=0.35$ as a function of temperature. Both the cell constant

TABLE I. Refined structural parameters from neutron powder-diffraction data for $La_{0.5}Sr_{1.5}Mn_{1-x}Ru_xO_4$. Space group $I4/mmm$. The atomic positions are La/Sr—$4e(0,0,z)$, Mn/Ru—$2a$ (0,0,0), O1—$4c$ (0,0.5,0), and O2—$4e$ (0,0,z).

x		0.1		0.2	0.35		0.5
Temperature		10 K	300 K	300 K	10 K	300 K	300 K
a (Å)		3.85983(3)	3.86729(4)	3.87421(4)	3.87033(4)	3.8797(1)	3.8843(1)
c (Å)		12.4165(2)	12.4422(2)	12.4776(2)	12.4898(2)	12.5113(5)	12.5368(3)
V (Å^3)		184.985(3)	186.085(4)	187.283(5)	187.091(5)	188.32(1)	189.147(6)
La/Sr	B_{iso} (Å^2)	0.10(2)	0.32(2)	0.59(3)	0.44(3)	0.75(3)	0.61(4)
	z	0.3581(1)	0.3581(1)	0.3581(1)	0.3578(1)	0.3578(1)	0.3575(1)
Mn/Ru	B_{iso} (Å^2)	0.18(6)	0.17(6)	0.4(1)	0.5(4)	0.5(4)	0.9(4)
	Occupancy	0.09	0.09(1)	0.17(1)	0.30	0.30(1)	0.41(1)
O1	B_{iso} (Å^2)	0.28(2)	0.66(3)	0.86(3)	0.65(3)	0.99(3)	0.93(4)
O2	B_{iso} (Å^2)	0.48(3)	0.93(3)	0.99(4)	0.84(4)	1.18(4)	1.07(5)
	z	0.1614(1)	0.1613(1)	0.1620(1)	0.1626(1)	0.1626(1)	0.1628(1)
R_p(%)		4.89	5.15	5.43	4.69	4.73	5.48
R_{wp}(%)		6.63	6.97	7.50	6.63	6.72	7.52
χ^2		3.23	2.67	2.32	2.42	2.43	3.04

and volume parameters decrease marginally with a decrease in the temperature. In the temperature range 10–300 K, the thermal contractions for the $x=0.1$ and 0.35 samples are -0.19% and -0.24% along the a axis, -0.21% and -0.17% along the c axis, and -0.59% and -0.65% in unit-cell volume, respectively. The reductions in the cell axes for $x=0.1$ are similar regardless of direction, while those for $x=0.35$ differ, signaling that the $x=0.35$ sample is more distorted. Interestingly, small anomalies near 80 K are observed in the lattice parameters, possibly associated with FM ordering induced by Ru doping. This will be addressed further in the discussion below.

Attempts to refine the neutron-diffraction data collected at temperatures below 80 K were not successful when only nuclear components were considered in the model. Although the predicted peak positions correlate well with those from the experiment, the calculated profiles are neither of the correct shape nor the correct intensity. Since any additional Bragg reflections due to a supercell or a change of symmetry were not detected, it is thus considered that the poor correlation is likely due to magnetic scatterings originating from the FM moments of the Mn/Ru sites. As is evident in Fig. 3, the calculated intensities of a (101) reflection for $x=0.35$ at

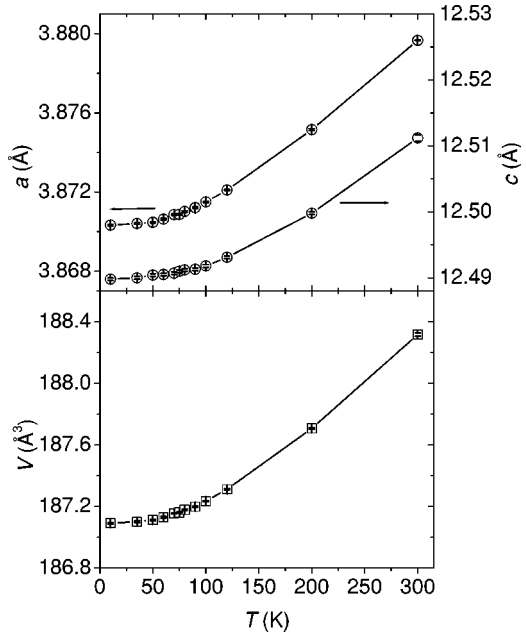

FIG. 2. Unit-cell parameters and volumes as a function of temperature for $x=0.35$.

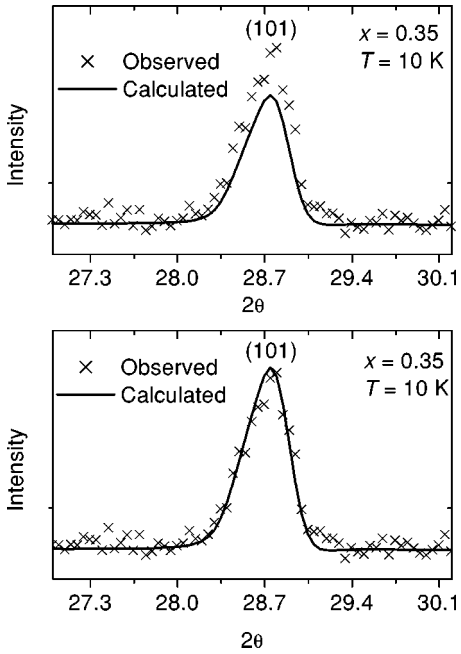

FIG. 3. Rietveld fit to the (101) reflection of $x=0.35$ at 10 K. The observed data are given as cross symbols and the fit is a solid line. The top panel displays the fit with a nuclear phase only. The figure in the bottom panel clearly demonstrates the improvement in the fit where both nuclear and magnetic reflections are considered.

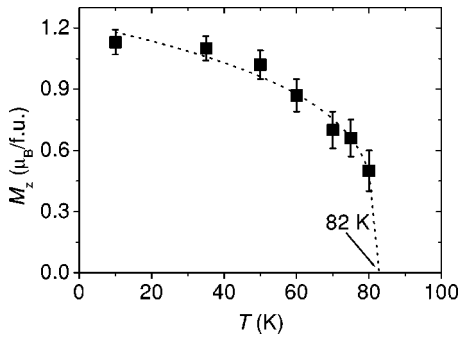

FIG. 4. Refined effective magnetic moment of the Mn/Ru sites versus temperature for $x=0.35$. Dotted lines are guides to the eye.

10 K better matched the experimentally observed values when the magnetic phase is included in the modeling. The top panel shows the fitted data with only a nuclear model, revealing the discrepancy between observed data points and simulated curve. The (101) peak presented in the bottom panel attests to the improvement of the fit. This provides direct evidence for the existence of long-range FM ordering in $x=0.35$, a conclusion further supported by the bulk magnetization data discussed below. A noteworthy feature is that the effective spins on the Mn/Ru sites are oriented predominantly along the z direction, which is in line with the observed uniaxial magnetic anisotropy in the $M(H)$ plot given in Fig. 7.

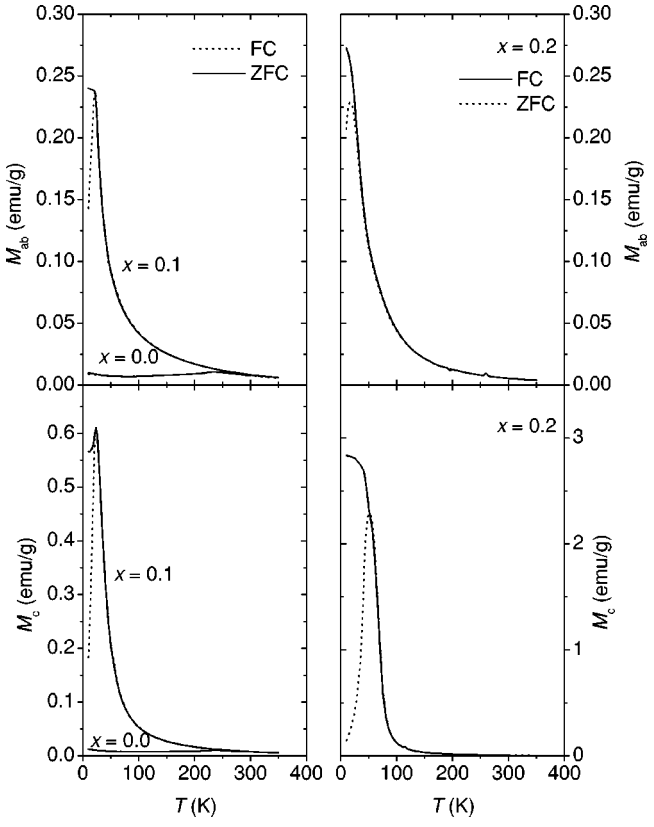

FIG. 5. Temperature dependence of the magnetization taken at 100 G for $x=0.0$ and 0.1 (left panel), and 0.2 (right panel). For the magnetization measurements, the field was applied parallel to the c axis, M_c, and the ab plane, M_{ab}. The top and bottom panels show M_{ab} and M_c as a function of temperature, respectively.

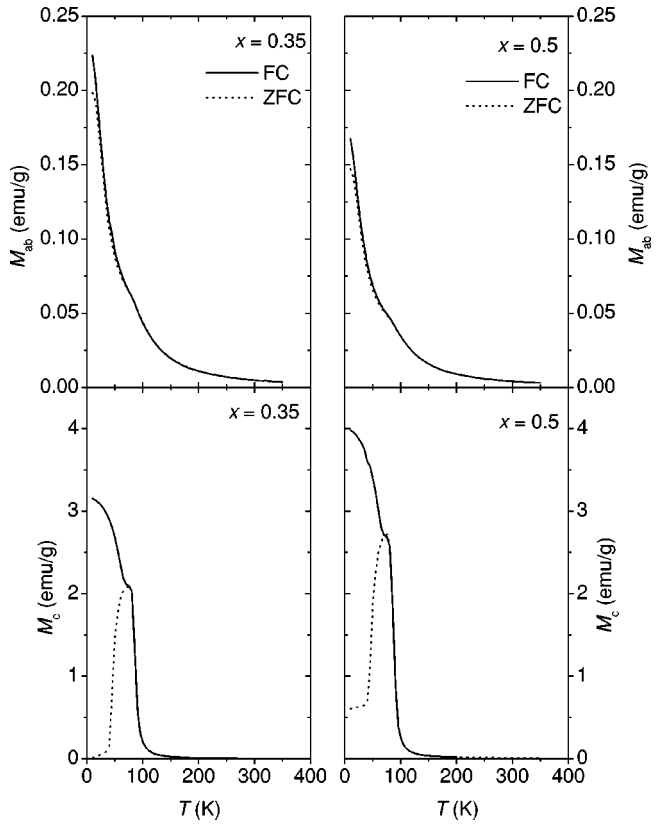

FIG. 6. Temperature dependence of the magnetization taken at 100 G for $x=0.35$ (left panel) and 0.5 (right panel). The top and bottom panels show the magnetization measured parallel to the ab plane and the c axis, respectively.

Figure 4 shows the magnetic moment on the Mn/Ru sites at selected temperatures refined from the neutron-diffraction data. The onset of long-range FM ordering for $x=0.35$ occurs at 82 K, which coincides with the Curie temperature in the $M(T)$ plot shown in Fig. 6. These results again illustrate that long-range FM order is truly operating in the 2D monolayered manganite system, despite the predictions of the isotropic Heisenberg model.[10] To the best of our knowledge, this is the first demonstrated case of spontaneous long-range FM ordering at zero field in a monolayered manganite system. Apparently, the Ru doping is the most likely cause of this observed FM ordering.

To elucidate the effect of the Ru doping on the material's magnetic properties, measurements were made of the temperature-dependent magnetization M of the Ru-doped crystals at 100 G for both zero-field-cooled and field-cooled runs. The magnetization measurements were made with magnetic fields parallel to both the c axis and the ab plane. The left panel of Fig. 5 shows the magnetization data for $x=0.0$ and 0.1, clearly revealing that the Ru doping makes the parent charge-ordered AFM phase develop a new FM moment regardless of field direction. For $x=0.1$, a typical spin-glass-like transition appears in the low-temperature region due to the competing interaction between the AFM and FM phases, which is supported by both frequency dependency

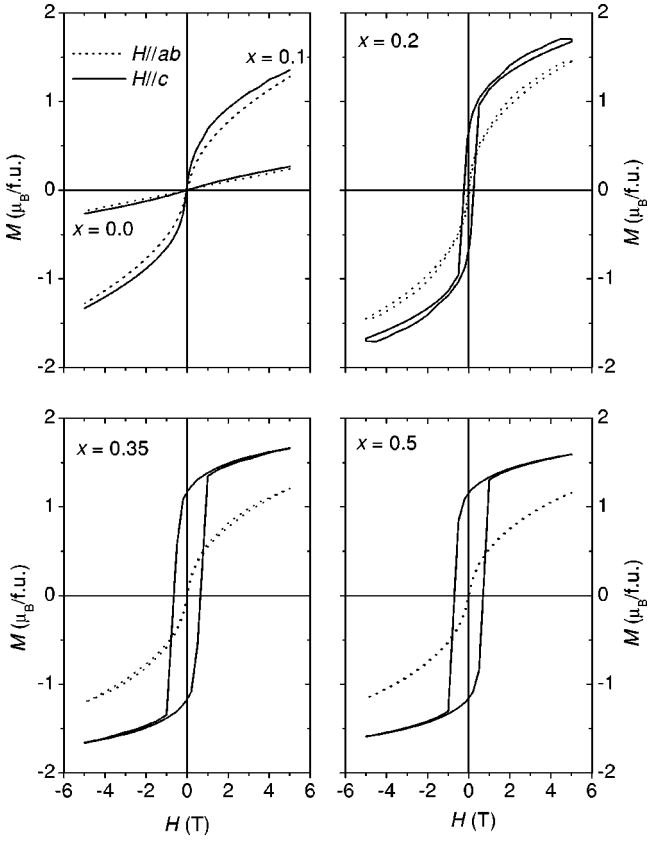

FIG. 7. Magnetization versus magnetic field for $x=0.0$, 0.1, 0.2, 0.35, and 0.5. The dashed line represents the $M(H)$ curve measured parallel to the ab plane. The solid line corresponds to the $M(H)$ curve measured along the c axis.

and memory effects.[20] A remarkable feature is that the magnitude of the magnetization strongly depends on the crystallographic axis. This anisotropic character becomes apparent in $x=0.2$, given in the right panel of Fig. 5, in which the magnitude of the axial magnetic moment M_c is roughly ten times that of the magnitude of the in-plane moment M_{ab}. The $M_c(T)$ curve displays a sharp magnetic transition (corresponding to the maximum in dM_c/dT) at 65 K.

As seen in the left panel of Fig. 6, for $x=0.35$ a clear FM transition along the c axis occurs at $T_C=85$ K, coinciding with the onset of long-range FM ordering as determined by the neutron-diffraction measurements. On the other hand, the $M_{ab}(T)$ curve does not show any noticeable evidence of FM ordering. This anisotropic magnetization is consistent with the spin direction obtained from the neutron-diffraction, which determined that the Mn/Ru spins were oriented along the c direction. The right panel of Fig. 6 reveals that the analogous anisotropic character induced by the Ru doping is observed in a more pronounced way in the $x=0.5$ sample, where FM ordering sets in at 86 K. The Weiss constant θ tends to increase with composition, indicating that the ferromagnetism in the system becomes pronounced with the Ru doping.

The field-dependent magnetization $M(H)$ data of the Ru-doped crystals taken at 10 K after zero-field cooling also show conspicuous anisotropic features with increasing values of x. As seen in Fig. 7, $M(H)$ for the $x=0.0$ sample is linearly dependent upon magnetic field, whereas for $x=0.1$ the new magnetic moment evolves at the expense of the charge-ordered AFM phase. As the Ru content increases, a marked difference between M_{ab} and M_c is found. The coercive fields H_C of $x=0.2$ are 330 G in the ab component and 2300 G along the c axis. For $x=0.35$, a huge coercivity of 6500 G exists along the c axis, relative to 150 G in the ab plane. The axial magnetization at 5 T is close to a value of $1.66\mu_B$, while the in-plane magnetization of $1.20\mu_B$ is higher as well. The $x=0.5$ compound possesses a H_C value of 6900 G along the c axis and 80 G in the ab plane. This salient feature of the behavior of H_C and $M_{5\,\mathrm{T}}$ for $x=0.5$ is reminiscent of uniaxial magnetic anisotropy—as predicted by Stoner-Wohlfarth model[21]—arising from the magnetic anisotropy of the Ru ion under the given crystal field.

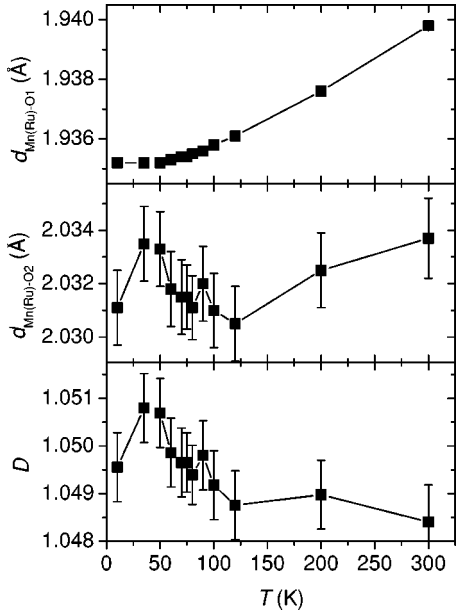

FIG. 8. Variations of Mn(Ru)-O1 and Mn(Ru)-O2 bond distances are shown in the top and middle panels as a function of temperature. The temperature dependent octahedral distortion D is given in the bottom panel. Solid lines are guides to the eye.

The anisotropic magnetic features found in the Ru-doped system appear to be related to the internal structural parameters of the material. As given in Fig. 8, there is a distinctive change in slope of the temperature-dependent variation of the axial Mn(Ru)-O2 bond length near T_C for the $x=0.35$ sample. On the other hand, the equatorial Mn(Ru)-O1 bond length gradually shortens with decreasing temperature. This change seemingly reflects in the octahedral distortion D defined as $d_{\mathrm{Mn(Ru)\text{-}O2}}/d_{\mathrm{Mn(Ru)\text{-}O1}}$, where $d_{\mathrm{Mn(Ru)\text{-}O1}}$ and $d_{\mathrm{Mn(Ru)\text{-}O2}}$ represent the equatorial and axial Mn(Ru)-O bond lengths, respectively. The D value also shows an abrupt increase below T_C, implying that the structural anisotropy becomes more prominent near the onset of FM ordering. This suggests that the ferromagnetism induced by Ru doping is associated with the observed structural anisotropy of the sample. An interesting feature in the bond-length data given in Table II is that the axial Mn(Ru)-O bond distance length-

TABLE II. Selected bond lengths (Å) for $La_{0.5}Sr_{1.5}Mn_{1-x}Ru_xO_4$.

x	0.1		0.2	0.35		0.5
Temperature	10 K	300 K	300 K	10 K	300 K	300 K
La(Sr)-O1	2.6134(5)×4	2.6182(7)×4	2.6243(8)×4	2.6263(8)×4	2.6323(8)×4	2.6387(10)×4
La(Sr)-O2	2.443(1)	2.450(2)	2.447(2)	2.438(2)	2.443(2)	2.441(2)
La(Sr)-O2	2.7399(1)×4	2.7452(1)×4	2.7510(2)×4	2.7486(2)×4	2.7551(2)×4	2.7584(2)×4
Mn(Ru)-O1	1.9299(1)×4	1.9336(1)×4	1.9371(1)×4	1.9352(1)×4	1.9398(1)×4	1.9421(1)×4
Mn(Ru)-O2	2.003(1)×2	2.006(1)×2	2.022(2)×2	2.031(1)×2	2.034(2)×2	2.042(2)×2

ens more rapidly with increasing Ru concentration than does the equatorial bond distance. Accordingly, the structure tends to be distorted more severely as x increases, as seen in Fig. 9. In fact, the variation in D correlates with the occurrence of the observed magnetic feature in this Ru-doped system. The increase in the structural distortion destroys the charge-ordered CE-type AFM framework that is normally present at lower D values, such as for $D=1.04$ for $La_{0.5}Sr_{1.5}MnO_4$.[22] Moreover, Mn spins in the perturbed AF matrix are easily reoriented antiparallel to adjacent Ru spins, as suggested by the $M(H)$ results. The magnetic anisotropy of the Ru ion is due to strong spin-orbit coupling under a given crystal field arising as a result of the structural anisotropy.

It is important to discuss the mechanism whereby Ru doping induces FM ordering in the AFM matrix. The parent material (for which $x=0.0$) has the CE- type AFM structure, which is composed of antiparallel FM zigzag chains. When $Ru^{4+}(t_{2g}^4)/Ru^{5+}(t_{2g}^3)$ replaces Mn^{4+} in the CE-type configuration, the structural parameters described above suggest that the Ru cation is surrounded by four Mn^{3+} ions in plane.[23] Two of them lie in the same FM chain and the other two are located in a neighboring FM chain. In the Ru-doped 3D perovskite manganites, $Ln_{0.4}Ca_{0.6}MnO_3$ (Ln = La, Pr, Nd, Sm) (Ref. 24) or $Sm_{1-x}Ca_xMnO_3$,[25] the FM superexchange interaction between the e_g orbital of Mn^{3+} and the vacant e_g orbital of Ru^{4+}/Ru^{5+} has been suggested as being responsible for the magnetic property. However, unlike the 3D system, the present 2D monolayered manganites $La_{0.5}Sr_{1.5}Mn_{1-x}Ru_xO_4$ exhibit prominent structural anisotropy, which causes breakdown of the e_g orbital degeneracy. The energy level of the d_{z^2} orbital will thus be lower than that of the $d_{x^2-y^2}$ orbital. This situation suggests that the magnetic d_{z^2} orbital of Mn^{3+} does not match in symmetry

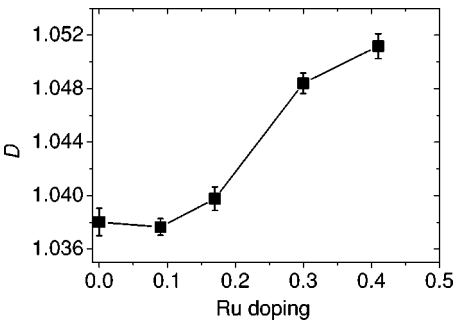

FIG. 9. Octahedral distortion as a function of the refined Ru doping concentration. Solid line is a guide to the eye.

the empty $d_{x^2-y^2}$ orbital of Ru^{4+} ion in the layer, preventing the FM interaction from developing. Instead, the d_π orbitals of the Ru ion are likely to interact antiferromagnetically with those of the four neighboring Mn ions via the superexchange pathway. Compared with the magnetic coupling of Mn-O-Mn, the exchange interaction of Ru-O-Mn will be stronger due to the diffusive nature of the $4d$ orbital of the Ru.[26] It is thus conceivable that the four neighboring Mn spins become antiparallel to the Ru spin. This proposed model is supported by $M(H)$ measurements and neutron data. First, the hysteresis observed at high fields in the $M(H)$ data of the $x \geqslant 0.2$ samples support the presence of the AFM couplings of Mn/Ru pairs. The magnitude of the irreversibility in the high-field region is inclined to decrease with increasing Ru doping, which can be attributed to the enhanced strength in AFM Mn/Ru couples due to the presence of further Ru neighbors for the Mn atom. Second, the neutron data for $x=0.35$ demonstrate that the magnetization value ($1.13\mu_B$) on the Mn/Ru site is much smaller than that ($>3\mu_B$) of the FM case among Mn/Ru, but closer to that ($2\mu_B$) of the AFM case. In the latter, the discrepancy might be due to the covalency effect of the Mn and Ru ions.[9] Accordingly, all four neighboring Mn spins around the Ru ion are ferromagnetically aligned. With increasing Ru concentration, the FM domains are extended, eventually leading to long-range ferromagnetism. This suggests that the Ru spin acts as a pinning center to control the spin direction of the neighboring Mn ions, generating the true long-range FM arrangement over the entire lattice.

The top panel of Fig. 10 displays the temperature dependence of normalized resistance parallel to the ab plane for the Ru-doped manganites, clearly revealing that with continued Ru doping the charge-ordered transition near 230 K completely disappears. This is likely through the destruction of the translational symmetry by Ru doping since, as its valence is 4+/5+ and its position is fixed, it will naturally lead to disappearance of any long-range charge order. The transport data are well fitted by the 2D variable-range hopping model,[15] defined as $\rho = A\exp(T_0/T)^{1/3}$, as shown in the inset of Fig. 10, but not at all well fitted when assuming a 3D model of conduction, implying that electrical conduction is confined to 2D layers in the material. The T_0 values obtained from the fit are 2.37×10^5 K for $x=0.2$, 1.86×10^5 K for $x=0.35$, and 1.40×10^5 K for $x=0.5$. These results indicate that localization lengths and hopping ranges are significantly enhanced with continued Ru doping, since localization length is proportional to $T_0^{-1/2}$.[15] Once more, this provides

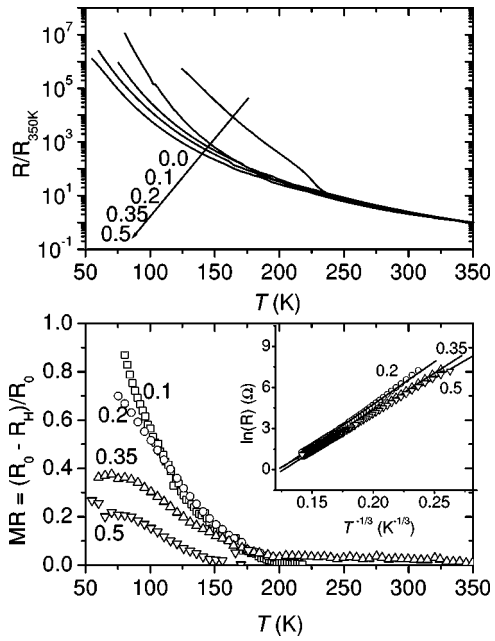

FIG. 10. Temperature dependence of in-plane normalized resistance for $x=0.0$, 0.1, 0.2, 0.35, and 0.5 is presented in the top panel. The bottom panel shows corresponding magnetoresistance (MR) curves. The inset is a plot of $\ln(R)$ vs $T^{-1/3}$. The solid line shows the best fit with the 2D variable-range hopping model.

evidence for the fact that Ru doping allows extended FM alignment at zero field.

The bottom panel of Fig. 10 shows the MR—defined as $(R_H\text{-}R_0)/R_0$—of the Ru-doped manganites, where R_0 stands for the resistance at 0 T and R_H at 5 T. Interestingly, MR is reduced as Ru concentration increases. This can be understood by carefully considering how the Ru doping suppresses the parent charge-ordered AFM phase and evolves a new FM phase. At $x=0.1$, the charge-ordered state begins to collapse and charge localization is relieved: namely, the spin-glass behavior evolves from the blended competition between the Mn and Ru spins. Application of the magnetic field to this frustrated system promotes the hopping of electrons due to field-induced spin alignment, affording high MR in the low-temperature region, consistent with the behavior of other magnetic glassy compounds, such as $(La_{2/3}Tb_{1/3})_{2/3}Ca_{1/3}MnO_3$ and $La_{2/3}Ca_{1/3}Mn_{1-x}Al_xO_3$.[27,28] Further Ru doping decreases the volume of magnetic glassy phase, but increases the volume of FM domains induced by the involvement of Ru atoms. At the sample composition of $x=0.35$, where long-range FM order is established, the MR is largely attributable to FM domains and their boundary effects. Since the pure FM alloy produces a tiny MR (2% for permalloy),[29] it is reasonable that the DE interaction contributed from Mn^{3+} and Mn^{4+} ions in the FM domains, together with the domain boundary effects, yields a relatively sizable MR of 40% at a low temperature. The $x=0.5$ sample has a smaller MR than the $x=0.35$ sample, which is due to the greater fraction of AFM Mn/Ru pairs in the lattice hindering the DE mechanism.

IV. CONCLUSION

Single crystals of the Ru-doped monolayered manganites $La_{0.5}Sr_{1.5}Mn_{1-x}Ru_xO_4$ $(0\leqslant x\leqslant 0.5)$ have been successfully grown using the floating-zone method. Ru doping at low concentrations induces a collapse in the charge-ordered phase and fosters the development of the spin-glass state. Remarkably, long-range FM ordering is observed in the high Ru-doped samples, even in the absence of a magnetic field. Until now, this has not been observed in monolayered manganite systems with a 2D structure. Furthermore, the uniaxial magnetic anisotropy also emerges in the high Ru-doped compounds. The magnetic anisotropy of the Ru ion associated with the structural anisotropy is the most likely causes of this unique magnetic behavior. The resistance data reveal that conduction routes are confined within the 2D layers of the material and the MR decreases with Ru doping, owing to the combined effect of magnetic glassy regions and FM domains. Accordingly, this study not only opens the possibility of discovering new CMR materials in the monolayered manganite system, but it also provides a better understanding of the underlying CMR mechanisms found in the layered manganite systems having a Ruddlesden-Popper-type structure.

ACKNOWLEDGMENTS

The authors thank Dr. E. O. Chi and Dr. J. Dho for their valuable discussion. The Creative Research Initiative Program provided financial support for this work.

*Corresponding author: nhhur@kriss.re.kr

[1] S. Jin, T.H. Tiefel, M. McCormack, R. A Fastnacht, R. Ramesh, and L.H. Chen, Science **264**, 413 (1994).

[2] Y. Tokura and N. Nagaosa, Science **288**, 462 (2000).

[3] P.M. Woodward, D.E. Cox, T. Vogt, C.N.R. Rao, and A.K. Cheetham, Chem. Mater. **11**, 3528 (1999).

[4] C.S. Hong, W.S. Kim, E.O. Chi, K.W. Lee, and N.H. Hur, Chem. Mater. **12**, 3509 (2000).

[5] C.N.R. Rao and A.K. Cheetham, Adv. Mater. (Weinheim, Ger.) **9**, 1009 (1997).

[6] Z. Zeng, M. Greenblatt, M.A. Subramanian, and M. Croft, Phys. Rev. Lett. **82**, 3164 (1999).

[7] E.J. Cussen, M.J. Rosseinsky, P.D. Battle, J.C. Burley, L.E. Spring, J.F. Vente, S.J. Blundell, A.I. Coldea, and J. Singleton, J. Am. Chem. Soc. **123**, 1111 (2001).

[8] Y. Sun, W. Tong, X. Xu, and Y. Zhang, Phys. Rev. B **63**, 174438 (2001).

[9] J.C. Burley, P.D. Battle, D.J. Gallon, J. Sloan, C.P. Grey, and M.J. Rosseinsky, J. Am. Chem. Soc. **124**, 620 (2002).

[10] N.D. Mermin and H. Wagner, Phys. Rev. Lett. **17**, 1133 (1966).

[11] C.S. Hong, J. Koo, S.-K. Son, Y.S. Lee, Y.-S. Kim, and Y. Do, Chem.-Eur. J. **7**, 4243 (2001).

[12] T. Kimura, K. Hatsuda, Y. Ueno, R. Kajimoto, H. Mochizuki, H. Yoshizawa, T. Nagai, Y. Matsui, A. Yamazaki, and Y. Tokura, Phys. Rev. B **65**, 020407(R) (2002).

[13] B.J. Sternlieb, J.P. Hill, U.C. Wildgruber, G.M. Luke, B. Na-

chumi, Y. Moritomo, and Y. Tokura, Phys. Rev. Lett. **76**, 2169 (1996).
[14] R. Ganguly, C. Martine, A. Maignan, M. Hervieu, and B. Raveau, Solid State Commun. **120**, 363 (2001).
[15] P.D. Battle, A.M.T. Bell, S.J. Blundell, A.I. Coldea, E.J. Cussen, G.C. Hardy, I.M. Marshall, M.J. Rosseinsky, and C.A. Steer, J. Am. Chem. Soc. **123**, 7610 (2001).
[16] C.S. Hong, E.O. Chi, W.S. Kim, N.H. Hur, and C.H. Lee, Chem. Mater. **13**, 945 (2001).
[17] C.S. Hong, W.S. Kim, E.O. Chi, N.H. Hur, and Y.N. Choi, Chem. Mater. **14**, 1832 (2002).
[18] T. He and R.J. Cava, Phys. Rev. B **63**, 172403 (2001).
[19] R.K. Sahu, Q. Mohammad, M.L. Rao, S.S. Manoharan, and A.K. Nigam, Appl. Phys. Lett. **80**, 88 (2002).
[20] Y. Moritomo, Y. Tomioka, A. Asamitsu, Y. Tokura, and Y. Matsui, Phys. Rev. B **51**, 3297 (1995).
[21] B. D. Cullity, *Introduction to Magnetic Materials* (Addison-Wesley, Philippines, 1972), p. 333.
[22] Y. Moritomo, A. Nakamura, S. Mori, N. Yamamoto, K. Ohoyama, and M. Ohashi, Phys. Rev. B **56**, 14 879 (1997).
[23] J.B. Goodenough, Phys. Rev. **100**, 564 (1955).
[24] B. Raveau, A. Maignan, C. Martin, R. Mahendiran, and M. Hervieu, J. Solid State Chem. **151**, 330 (2000).
[25] C. Martin, A. Maignan, M. Hervieu, C. Autret, B. Raveau, and D. Khomskii, Phys. Rev. B **63**, 174402 (2001).
[26] M.P. Shores, J.J. Sokol, and J.R. Long, J. Am. Chem. Soc. **124**, 2279 (2002).
[27] J.M. De Teresa, M.R. Ibarra, J. Garcia, J. Blasco, C. Ritter, P.A. Algarabel, C. Marquina, and A. del Moral, Phys. Rev. Lett. **76**, 3392 (1996).
[28] J. Blasco, J. Garcia, J.M. de Teresa, M.R. Ibarra, J. Perez, P.A. Algarabel, C. Marquina, and C. Ritter, Phys. Rev. B **55**, 8905 (1997).
[29] C. Tsang, H. Santini, D. McCown, J. Lo, and R. Lee, IEEE Trans. Magn. **32**, 7 (1996).